THE JOURNAL OF BIOLOGICAL CHEMISTRY VOL. 283, NO. 27, pp. 18685–18693, July 4, 2008
© 2008 by The American Society for Biochemistry and Molecular Biology, Inc. Printed in the U.S.A.

GIT1 Paxillin-binding Domain Is a Four-helix Bundle, and It Binds to Both Paxillin LD2 and LD4 Motifs*[S]

Received for publication, February 19, 2008, and in revised form, April 8, 2008 Published, JBC Papers in Press, April 30, 2008, DOI 10.1074/jbc.M801274200

Ziwei M. Zhang[‡§], Joseph A. Simmerman[‡1], Cristina D. Guibao[‡], and Jie J. Zheng[‡§2]

From the [‡]Department of Structural Biology, St. Jude Children's Research Hospital, Memphis, Tennessee 38105 and the [§]Department of Molecular Sciences, University of Tennessee Health Science Center, Memphis, Tennessee 38163

The G protein-coupled receptor kinase-interacting protein 1 (GIT1) is a multidomain protein that plays an important role in cell adhesion, motility, cytoskeletal remodeling, and membrane trafficking. GIT1 mediates the localization of the p21-activated kinase (PAK) and PAK-interactive exchange factor to focal adhesions, and its activation is regulated by the interaction between its C-terminal paxillin-binding domain (PBD) and the LD motifs of paxillin. In this study, we determined the solution structure of rat GIT1 PBD by NMR spectroscopy. The PBD folds into a four-helix bundle, which is structurally similar to the focal adhesion targeting and vinculin tail domains. Previous studies showed that GIT1 interacts with paxillin through the LD4 motif. Here, we demonstrated that in addition to the LD4 motif, the GIT1 PBD can also bind to the paxillin LD2 motif, and both LD2 and LD4 motifs competitively target the same site on the PBD surface. We also revealed that paxillin Ser^{272} phosphorylation does not influence GIT1 PBD binding *in vitro*. These results are in agreement with the notion that phosphorylation of paxillin Ser^{272} plays an essential role in regulating focal adhesion turnover.

Cells attach and communicate with the extracellular matrix through membrane peripheral proteins that form focal adhesions (FAs)[3] (1, 2). Cell motility is regulated through the alternative assembly and disassembly of FAs and cytoskeletal proteins (3). The dynamics of FAs are controlled by the signaling of different adhesion molecules such as focal adhesion kinase (FAK), paxillin, the G protein-coupled kinase-interacting (GIT) protein, and p21-activated kinase (PAK) (4–7), whereas cytoskeletal remodeling is regulated by small GTPases of the Ras and Rho family, such as Rac1, Cdc42, and RhoA (8–10).

GIT proteins play an important role in initiating the disassembly of FAs (11, 12). Both members of the GIT protein family, GIT1 and GIT2/p95-PKL, have an N-terminal Arf GTPase-activating protein domain, a Spa2-homology domain, a coiled-coil domain, and a C-terminal paxillin-binding domain (PBD). Previous studies have shown that the Spa2 homology domain binds the PAK·PIX complex, and the PBD binds paxillin (11, 13–15). GITs, functioning as scaffold proteins, target the PAK complex into FAs by binding with paxillin via their PBDs (11, 13, 16). GIT PBDs span about 130 amino acids and are highly conserved among species (17). Recently, a low-resolution structural model for the GIT1 PBD was derived from small-angle x-ray scattering and homology modeling, based on the structure of the FAK focal adhesion targeting (FAT) domain, which is a four-helix bundle protein (15). Mutagenesis studies suggest that paxillin binds the GIT1 PBD through the putative helices H1 and H4 (15). However, a high-resolution structure of the GIT1 PBD is unavailable, and the mechanism of paxillin-GIT interaction remains unclear.

Paxillin is one of the major binding partners of GIT proteins in FAs, functioning as an elongated adaptor protein that links actin filaments with integrin (18). It contains multiple docking sites for different signaling and structural proteins in FAs and comprises five N-terminal LD motifs and four C-terminal LIM domains (19, 20). The LD motifs are named after their consensus sequence LD*X*LL*XX*L and bind with multiple proteins, including FAK, GIT, vinculin, actopaxin, and integrin-linked kinase (13, 21–23). Structural studies have shown that the LD2 motif and the bound form of the LD4 motif form amphipathic α-helices, with several leucines forming a large hydrophobic patch (24, 25). FAK interacts with paxillin on both LD2 and LD4 motifs (23, 26). Unlike FAK, the interaction between GIT1 and paxillin is reported to be mediated by the LD4 motif only (13, 14).

In this study, we determined the solution structure of the PBD of rat GIT1 (residues 640–770) by NMR spectroscopy. Using synthesized LD peptides, we also studied the interaction between the GIT1 PBD and paxillin LD motifs. Our finding reconciles some controversial observations of earlier studies and provides a clearer picture of the role of GIT proteins in focal adhesion regulation.

* This work was supported, in whole or in part, by National Institutes of Health Grant R01GM069916. This work was also supported by the American Lebanese Syrian Associated Charities. The costs of publication of this article were defrayed in part by the payment of page charges. This article must therefore be hereby marked "*advertisement*" in accordance with 18 U.S.C. Section 1734 solely to indicate this fact.

[S] The on-line version of this article (available at http://www.jbc.org) contains supplemental Figs. S1–S8.

The atomic coordinates and structure factors (code 2JX0) have been deposited in the Protein Data Bank, Research Collaboratory for Structural Bioinformatics, Rutgers University, New Brunswick, NJ (http://www.rcsb.org/).

[1] Present address: Dept. of Cellular and Molecular Biology, Adam State College, Alamosa, CO 81102.

[2] To whom correspondence should be addressed: Dept. of Structural Biology, St. Jude Children's Research Hospital, 332 N. Lauderdale St., Memphis, TN 38105. Tel.: 901-495-3168; Fax: 901-495-3032; E-mail: jie.zheng@stjude.org.

[3] The abbreviations used are: FA, focal adhesion; FAK, FA kinase; PAK, p21-activated kinase; PIX, PAK-interactive exchange factor; PBD, paxillin-binding domain; GIT, G protein-coupled kinase-interacting; FAT, focal adhesion targeting; Vt, vinculin tail; MOPS, 3-(*N*-morpholino)propanesulfonic acid; HSQC, heteronuclear single-quantum coherence; NOE, nuclear Overhauser effect.

EXPERIMENTAL PROCEDURES

Protein Purification and Peptide Synthesis—Full-length rat GIT1 cDNA was a gift from Dr. Edward Manser. The sequence of rat GIT1 is identical to human GIT1 sequence except for one substitution (P644L) in the N-terminal unstructured region. We subcloned the GIT1 PBD (residues 640–770) into the pET28 vector (EMD Biosciences, San Diego, CA). The protein was overexpressed in *Escherichia coli* strain BL21(DE3). The $^{13}C/^{15}N$-labeled sample was prepared by growing the cells in MOPS-buffered medium containing $^{15}NH_4Cl$ (1 g/liter) and [$^{13}C_6$]glucose (3.6 g/liter) (27). Proteins were purified using Ni^{2+}-charged His-Bind resins (EMD Biosciences) according to the manufacturer's protocol. The His_6 tag was removed by thrombin cleavage (EMD Biosciences) at room temperature for 4 h. The digested protein was dialyzed in 20 mM potassium phosphate (pH 6.5), 5 mM 1,4-dithiothreitol, and 5 mM EDTA and then further purified by gel filtration on a HiLoad 26/60 Superdex 75 HR column (GE Healthcare). Human paxillin LD2 (residues 140–161), LD4 (residues 261–282), and the LD4 peptide phosphorylated at Ser^{272} were chemically synthesized and purified by high pressure liquid chromatography at the Hartwell Center of Bioinformatics and Biotechnology.

NMR Spectroscopy—The $^{15}N/^{13}C$-double-labeled GIT1 PBD sample used for structure determination was ~400 μl at a concentration of 1.2 mM in 20 mM potassium phosphate buffer (pH 6.5), 5 mM deuterated EDTA, 5 mM deuterated dithiothreitol, and 5% (v/v) D_2O. All NMR spectra for structure determination were acquired at 37 °C with a Bruker Avance 600 or 800 MHz spectrometer equipped with a cryoprobe. To determine the residues exposed to the solvent, a ^{15}N-labeled GIT1 PBD sample was first lyophilized in a Labconco FreeZone Plus 6 freeze dry system (Labconco Corp., Kansas City, MO) and dissolved in the same volume (400 μl) of D_2O. ^{15}N heteronuclear single-quantum coherence (HSQC) spectra were collected at 25 °C every 10 min by the Bruker 600 MHz spectrometer. Spectra were analyzed by the software Sparky (28).

NMR Data Analysis and Structure Calculation—All NMR spectra were processed with NMRPipe (29) and analyzed with CARA (30). Backbone assignments were obtained based on CBCA(CO)NH, HNCACB, HNCA, and HN(CO)CA experiments. Side chain assignments were obtained by using HCCH-TOCSY, HCCH-COSY, HBHA(CO)NH, CC(CO)NH, and HCC(CO)NH spectra. Dihedral angle range was predicted by TALOS (31). For structural determination, the nuclear Overhauser effect (NOE) distance restraints were derived from ^{13}C and ^{15}N NOESY spectra. NOE spectra were first analyzed by an automatic algorithm with the software ATNOS/CANDID (32, 33), and the results were then manually inspected and modified. Structure calculation and refinement were carried out by using the software CYANA 2.1 (34). The final structures were checked and validated by PROCHECK (35). Structure figures in this paper are generated by Molmol (36). For the electrostatic potential map, the figure was generated by Pymol, based on the electrostatic potential generated by GRASP (37). The structure superposition and structure-based sequence alignment are generated by the Swiss-PdbViewer (38).

Chemical Shift Perturbation Titration—All NMR titration experiments were performed at 25 °C under the same conditions: ^{15}N-labeled GIT1 PBD at a concentration of 400–450 μM in 20 mM potassium phosphate (pH 6.5), 5 mM deuterated EDTA, 5 mM deuterated dithiothreitol, and 5% (v/v) D_2O. All peptide stocks were prepared in the same buffer, and their pH was readjusted to 6.5 before titration. Titrations were made by adding ligand at the following ratios: 1:0.5, 1:1, 1:2, and 1:5. A series of ^{15}N HSQC spectra were taken on a Bruker Avance 600 MHz spectrometer with a cryoprobe, and data were analyzed with Sparky (28).

Biacore Binding Assay—Synthesized LD peptides with the N-terminal biotin tag were attached to a NeutrAvidin-covered gold surface (CM5 chip, GE Healthcare). Kinetic studies were performed at 20 °C with a Biacore 3000 (GE Healthcare). The purified GIT1 protein (in 20 mM phosphate buffer (pH 6.5), 150 mM NaCl, 5 mM EDTA, 0.1 mg/ml bovine serum albumin, and 0.005% P20 surfactant) was injected to flow through the chip, and K_d was derived by fitting the data from three injections. The association and dissociation were observed at a flow rate of 50 μl/min in a concentration range of 1.4–110 μM. Binding affinities were determined by the program Scrubber 2 (version 2.0b, BioLogic Software). The experiment was repeated with chips covered with both high- and low-density peptides, and the results were found to be compatible.

CD Spectroscopy—All CD spectra were obtained with an Aviv 62DS CD spectrometer (Aviv, Lakewood, NJ). The CD spectrum of the PBD was taken at 25 °C in 50 mM potassium phosphate (pH 6.5) and 1 mM EDTA. The thermostability of the protein was determined by monitoring the CD signal of the PBD sample at 222 nm while increasing the sample temperature.

RESULTS

Solution Structure of the GIT1 PBD Is a Four-helix Bundle—The PBD of rat GIT1 (residues 640–770) (Fig. 1*a*) was expressed in *E. coli* as a soluble protein, and CD spectroscopy showed that the protein was predominantly helical. The CD studies also showed that the protein was relatively stable, and it started to unfold at about 45 °C (supplemental Fig. S1). The solution structure of the PBD was determined by heteronuclear multidimensional NMR spectroscopy. After backbone and side chain assignments, the NOE constraints were obtained from both ^{15}N- and $^{15}N/^{13}C$-edited three-dimensional NOESY spectra. The structure of the PBD was determined based on 2440 NOE distance constraints and 189 dihedral angle constraints. The structures were calculated by CYANA, and 20 structures with the lowest target function value were selected and superimposed (Fig. 1*b*). Table 1 gives the final structural statistics. All experimental NMR constraints were satisfied, the average target function of the 20 structures selected is 0.7, and no NOE constraint violation was >0.2 Å. Most residues (81%) had dihedral angles in the most favored region of the Ramachandran plot, and 10.9% residues are in the additionally allowed region. The only residue in the disallowed region was Asp^{643}, which is located in the unstructured N terminus. The solution structure was of high precision. The average root mean square deviations of the 20 structures from the average structure for backbone atoms and

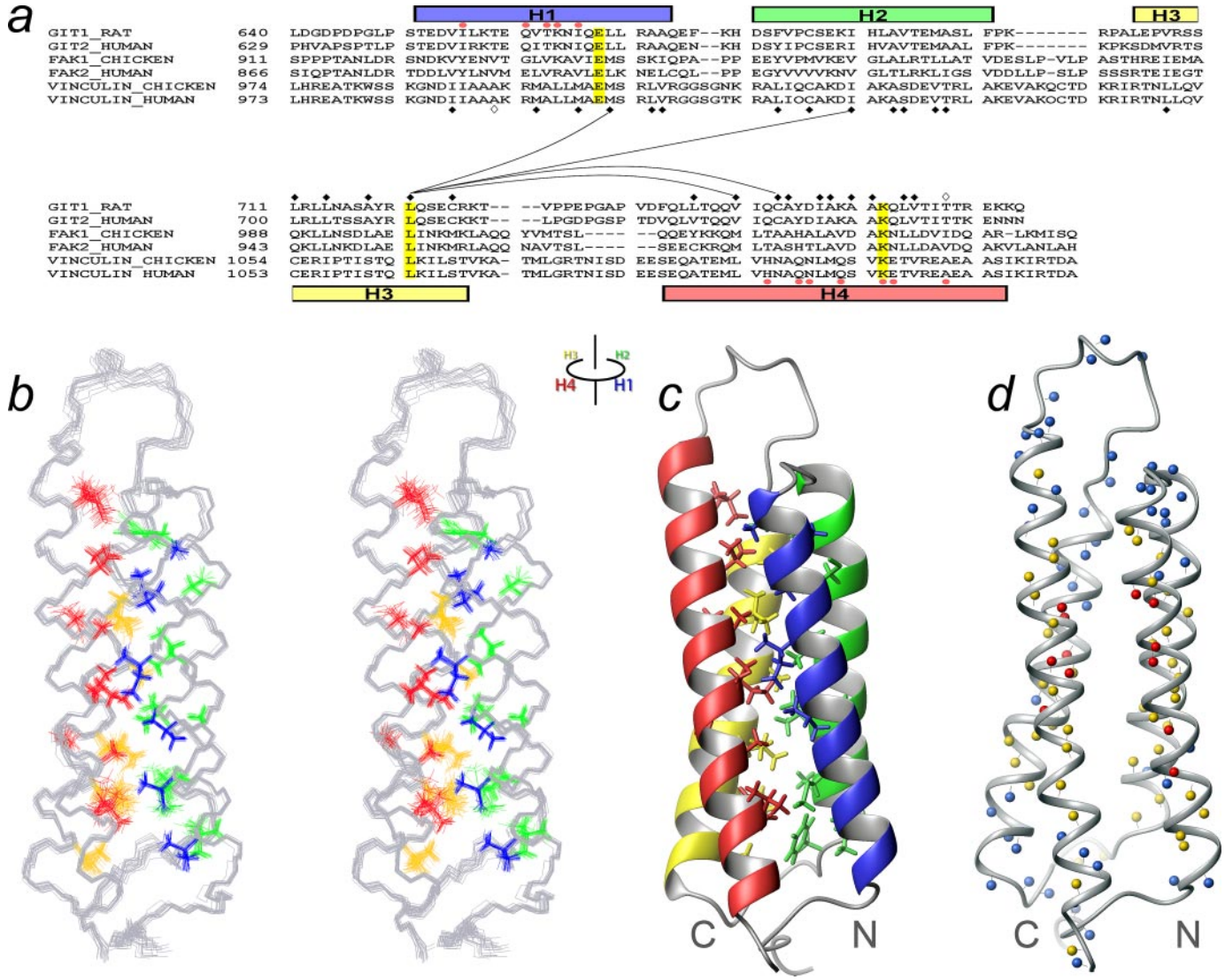

FIGURE 1. **Structure of the PBD of rat GIT1.** *a*, sequence alignment based on structures of the rat GIT1 PBD, the chicken FAK FAT domain (Protein Data Bank code 1KTM), and H2 to H5 of the chicken Vt domain (code 1QKR). The sequences of human GIT2, FAK2/PYK2, and vinculin are also aligned based on the structure-based sequence alignment. Residues that are significantly perturbed by the binding of LD peptides are indicated with *red dots*. The hydrophobic core is composed of residues marked by *filled diamonds*. Hydrophobic residues are marked by *filled diamonds*, and the two polar Ts are marked by *open diamonds*. The absolutely conserved residues are highlighted in *yellow*. *b*, stereo view of the backbone trace of the ensemble of the 20 best structures. The side chain of the hydrophobic core is shown. *c*, ribbon representation of the GIT1 PBD structure. H1 to H4 are shown in *blue*, *green*, *yellow*, and *red*, respectively. Side chains of the interlaced core are also presented. *d*, representation of the H/D exchange experiments. The unambiguously observed non-proline amide proton atoms are represented as small *balls* in the structure. After the first 15 min, the solvent-exchanged amide proton atoms are colored in *blue*, whereas the protected amide protons are colored in *yellow*. The atoms that remain protected after 380 min are colored in *red*.

all heavy atoms of residues 643–767 were 0.39 and 0.77 Å, respectively. The coordinates and the structure factors of the GIT1 PBD have been deposited in the Protein Data Bank with accession code 2JX0.

The GIT1 PBD forms a compact rod-shaped protein with a well defined C terminus and a slightly floppy N terminus. The C-terminal end is in proximity to the N terminus, a feature common to many functional independent domains. The PBD structure forms a four-helix bundle with a right-handed up-and-down topology, about 58 Å in height and 26 Å in diameter (Fig. 1*c*). The four helices form an antiparallel bundle, with many NOEs observed between helix turns and an average axis angle of 19.1° between neighboring helices. The hydrophobic side chains from all helices interlace to form a network of hydrophobic interactions that dramatically stabilize the bundle (Fig. 1, *b* and *c*). Extensive interhelical NOEs were observed, resulting in well defined side chains of the residues located in the interhelical regions (Fig. 1*c*).

The PBD fold was confirmed by the solvent-exposed surface mapped by the hydrogen/deuterium (H/D) exchange experiments. Fast ^{15}N HSQC spectra were taken immediately after dissolving the lyophilized ^{15}N-labeled PBD in D_2O. After the first 15 min, ~57% of amide peaks had disappeared because of H/D exchange. All the protected peaks were in the helical regions, whereas most peaks that vanished belonged to the residues in the loop regions and the termini (Fig. 1*d*). Some peaks were protected even after 6 h; they were all within the core of the four-helix bundle. The H/D exchange data validates the 81 pairs of H-bonds in the structure, most of which were between O_i and HN_{i+4} from individual helices.

TABLE 1
Statistics of the GIT1 PBD structure determined by NMR spectroscopy

Distance restraints	
Total no. of NOE restraints	2440
Intraresidue	574
Sequential	750
Medium range	718
Long range	398
Restraints per residue	18.07
Dihedral angle restraints	
Total number of restraints	189
ϕ angle restraints	93
ψ angle restraints	96
Ramachandran plot (%)	
Residues in most favored regions	88.1
Residues in additional allowed regions	10.9
Residues in generously allowed regions	0.5
Residues in disallowed regions	0.4
r.m.s.d.[a] (residues 643–767; Å)	
Average backbone r.m.s.d. to mean	0.39 ± 0.09
Average heavy atom r.m.s.d. to mean	0.77 ± 0.07
Target function	0.70 ± 0.04

[a] r.m.s.d., root mean square deviation.

Of the four helices in the PBD structure, H4 (30 residues) is slightly longer than helices H1 (23 residues), H2 (21 residues), and H3 (22 residues). The H3/H4 loop is longer than the H1/H2 loop, which may explain why H3 and H4 appear longer than H1 and H2 in the low-resolution small-angle x-ray scattering model (15). The GIT1 PBD had 11 prolines, all located in the loops or at the end of helices. The rigid backbone and hydrophobic side chain of proline make the loops less flexible, allowing us to observe extensive NOE connections between the loops and the rest of the protein. The PBD also has three cystines; the chemical shifts of C-β of all three cystines were less than 32 ppm, indicating that they were in the reduced forms (39). This might be caused by the presence of 5 mM dithiothreitol in the NMR sample buffer. In the solution structure, Cys^{683} and Cys^{725} are closely located in helices H2 and H3, and the distance between the C-α atoms of the two residues is 8.7 Å. A small degree of rotation of the Cys^{683} side chain or a slight change in the packing of the helices can bring the two cysteine side chains close enough to form a disulfide bond. Considering the high thermostability of the PBD, we cannot rule out the possibility of a disulfide bond bridge between the two cysteines.

A sequence comparison of the GIT1 PBD with those of two other four-helix bundle domains, the FAT domain of FAK and the vinculin tail (Vt) domain, revealed that the hydrophobic residues in the core regions that hold the four helices together are well conserved among all three sequences (Fig. 1*a*). The best example of the hydrophobic residues is Leu^{721} in helix H3, wherein the side chain of the residue had hydrophobic contacts with side chains of Leu^{668}, Ile^{687}, Val^{746}, and Cys^{749} (supplemental Fig. S2). In the structure-based sequence alignment, not only was Leu^{721} conserved among the three domains, but the residues that had hydrophobic contacts with this leucine were well conserved too. Although different in surface residues, the three domains share a conserved central hydrophobic network that holds the bundle together. The overall folding of the GIT1 PBD is very similar to that of the FAT domain of FAK (root mean square deviation value of 1.65 Å) and helices H2 to H5 of the Vt domain (root mean square deviation value of 1.68 Å calculated and averaged on C-α pairs) (supplemental Fig. S3). The Vt domain is a five-helix bundle, with the first helix attached to the groove between helices H2 and H5. The distance between Vt H2 and H5 is slightly more than that between GIT1 H1 and H4, probably because Vt H1 is attached to the groove.

It has been demonstrated that the FAK FAT domain features helix H1 swapping dynamics and dimer formation (25, 40), although the biological importance of such a dimer in the context of full-length FAK is not very clear. However, unlike the FAT domain, our NMR data clearly indicated that PBD existed as a monomer in solution. In addition, the ^{15}N HSQC spectrum of the PBD taken at 37 °C revealed that all amide peaks of the protein had similar intensity, suggesting that the PBD has few flexible loops. Also, a change of sample temperature from 37 to 13 °C resulted in a series of spectra showing all peaks with unchanged intensities; no local line broadening was observed when decreasing temperature (supplemental Fig. S4), further suggesting that the PBD was a rigid protein. It is likely that such difference in the two proteins was caused by the sequence of the loop that linked helices H1 and H2, the H1/H2 loop. In the PBD, the sequence of this loop is EFKH, whereas the equivalent loop in the FAT domain is PAPP; the three prolines in the FAT domain probably introduce the conformational strain that probably triggers the helix H1 swapping dynamics observed in the FAT domain.

The PBD and the FAT Domain Are Similar on the H1/H4 Surface but Different on the H2/H3 Surface—Forming four amphipathic helices, the GIT1 PBD buries most of its hydrophobic side chains in the bundle core. There is only one major hydrophobic patch on the surface. As shown in Fig. 2*a*, side chains from H1 and H4 form two positive-charged ridges sandwiching an elongated hydrophobic groove, which covers about two-thirds of the bundle length. To the center of the H1/H4 surface, positively charged Lys^{663}, Lys^{755}, and Lys^{758}, and polar residues Thr^{662}, Gln^{666}, and Tyr^{751} enclose a well defined hydrophobic pocket composed of Ile^{665}, Ala^{754}, and Ala^{757} at the bottom. These residues are conserved between GIT1 and GIT2 in all organisms for whom sequences are available. Among them, Lys^{663}, Lys^{758}, Ala^{754}, and Ala^{757} are also conserved with the FAK FAT domain, with a conserved Ile^{665}/Val^{936} substitution (Fig. 1*a*). This surface makes an ideal binding site for paxillin, as confirmed by chemical shift perturbation titration experiments.

When the GIT1 PBD was compared with the FAT domain of FAK, the latter had two major hydrophobic grooves located at both the H1/H4 and H2/H3 faces, which correspond to the LD2 and LD4 motif binding sites, respectively (41) (Fig. 2*b*). Both grooves have a surface setting similar to that of the H1/H4 site of the PBD: a hydrophobic groove with surrounding polar and positive-charged ridges. Structural superimposition of the PBD and the FAT domain revealed that GIT1 Lys^{663}/FAK Lys^{934} and GIT1 Lys^{758}/FAK Lys^{1033} were in the same position, which is another indication of functional similarity arising from structural similarity. The electrostatic interaction between the side chain of FAK Lys^{1033} and the conserved Asp^{146} in the LD2 motif might be important in determining binding specificity. Thus, we speculated that the analogous Lys^{663} and Lys^{758} in GIT1

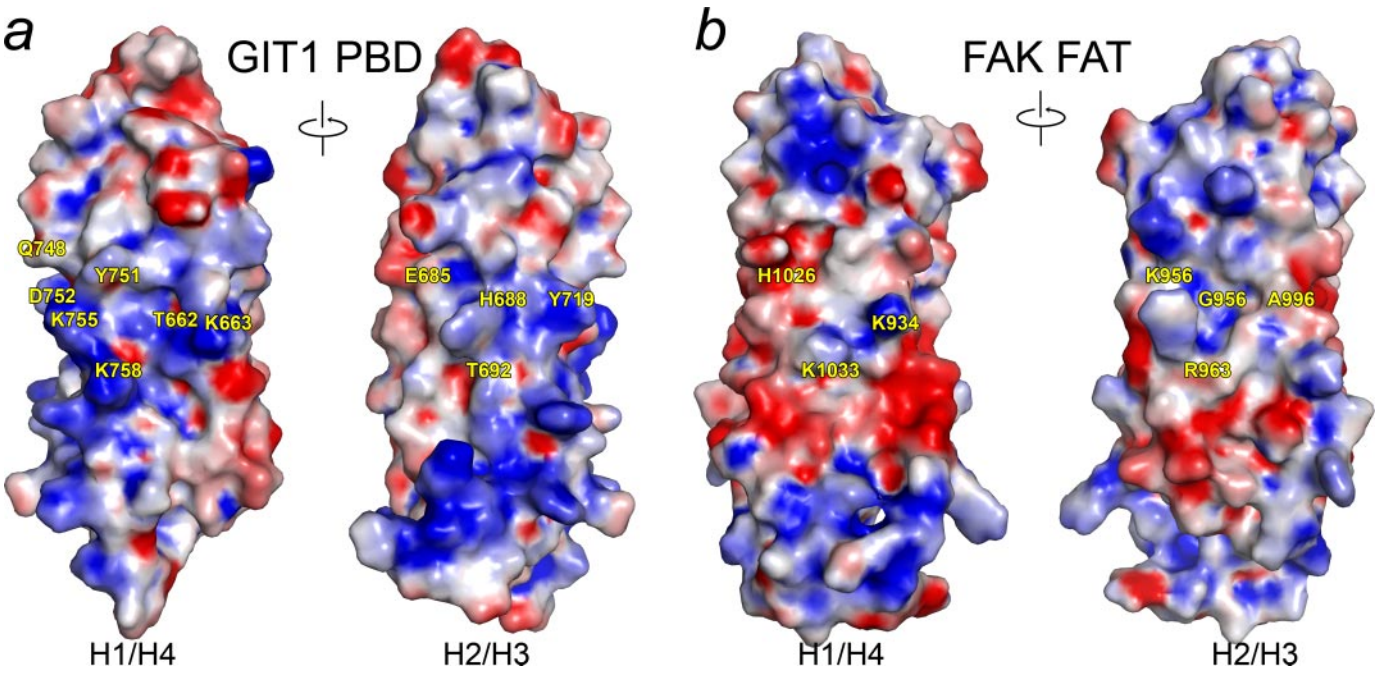

FIGURE 2. **Electrostatic surfaces of PBD and FAT domains.** Positive charge is shown in *blue* and negative charge in *red*. Equivalent residues are marked in both structures. The residues that exhibited the most significant perturbations during LD peptide titrations are labeled on the GIT1 H1/H4 surface. The figure was generated by Pymol, based on the electrostatic potential generated by GRASP.

might also greatly contribute to paxillin binding; this prediction was confirmed by the studies described in the next section.

The FAT surface has two hydrophobic surfaces that serve as LD motif binding sites, but the GIT1 PBD has only one such surface (Fig. 2). In the FAT domain, helices H2 and H3 form a second hydrophobic surface, and at the center of the FAT H2/H3 site, the bottom of the hydrophobic pocket is composed of Gly^{959} and Ala^{996} on H2 and H3, respectively. However, the equivalent position on GIT1 PBD is occupied by bulky His^{688} and Tyr^{719}, which effectively close the pocket. Moreover, the positively charged H2 ridge in the FAT domain is also eliminated by the substitutions of Lys^{956} and Arg^{963} in FAK by Glu^{685} and Thr^{692} in GIT1. Interestingly, we found that the Vt domain was more similar to FAK; for example, FAK Lys^{956} was conserved as Lys^{1021} in the Vt domain, whereas FAK Gly^{959} was substituted with a small residue Ala^{1024} in the Vt. This suggests a possible paxillin binding site on the H2/H3 surface of the Vt domain.

Paxillin LD4 Motif Binds to the PBD at the H1/H4 Face—The binding between the GIT1 PBD and paxillin is essential to localize the PAK·PIX·GIT complex to the focal adhesion (42). Although the interaction between the paxillin LD4 motif and GIT proteins had been proposed (11, 13, 14), the details about the binding remained unknown. Therefore, we analyzed the interaction between the GIT1 PBD and the paxillin LD4 motif by chemical shift perturbation experiments (Fig. 3*a*). In the experiments, we used a peptide comprising the LD4 motif of paxillin (residues 261–282, designated LD4 peptide (Fig. 3*c*) to titrate the ^{15}N-labeled PBD and found that the LD4 peptide bound to the PBD on the H1/H4 surface. The binding site was located to the central region of the H1 and H4 solvent-exposed surface, corresponding to the two clusters of largely shifted peaks in the perturbation plot (Fig. 3*d*). Although the two clusters seemed to be remote in the sequence of the PBD, they were actually in close contact in the three-dimensional structure, forming the two ridges and the hydrophobic pocket mentioned previously (Fig. 2*a*).

Most of the shifted peaks affected by the bound LD4 peptide were in the intermediate exchange time scale. Additionally, the cluster in H4 was higher than that in H1 in average, indicating a slightly stronger association with H4 than H1 (Fig. 3*d*). The solvent-exposed Thr^{662}, Lys^{663}, Gln^{748}, Tyr^{751}, Asp^{752}, Lys^{755}, and Lys^{758} exhibited significant perturbations (Lys^{633}, Tyr^{751}, and Lys^{758} had the largest perturbations as shown in Fig. 3, *a* and *d*), whereas the residues between them, which were buried between the helices, showed only moderate changes. This indicates that the large shift is not due to a binding-induced conformational change. The cluster in H1 corresponded to the paxillin-binding sequence 2 (PBS2) proposed by sequence analysis (13). Compared with the H1/H4 site, residues in H2 and H3 had only minimal or moderate shifts on LD4 peptide titration. A closer inspection of the shifted peaks in H2 and H3 showed that most peaks were residues at the interface with H1 or H4, and among those, buried residues showed more perturbation than exposed ones, indicating that the perturbation was due to proximity to the H1/H4 binding site. These data are in agreement with a recent mutagenesis study that showed the mutations within H2 and H3 did not influence paxillin binding, whereas the mutations in H1 and H4 decreased paxillin binding; especially the K663E and K758E mutations substantially decreased paxillin association (15).

The Effect of Paxillin Ser^{272} Phosphorylation on the Binding of GIT1 PBD—It was reported that paxillin Ser^{272} (Ser^{273} in chicken sequence) phosphorylation promoted GIT1 focal adhesion localization in cells (12), so we wanted to investigate the interaction with GIT1 and phosphorylated paxillin. We

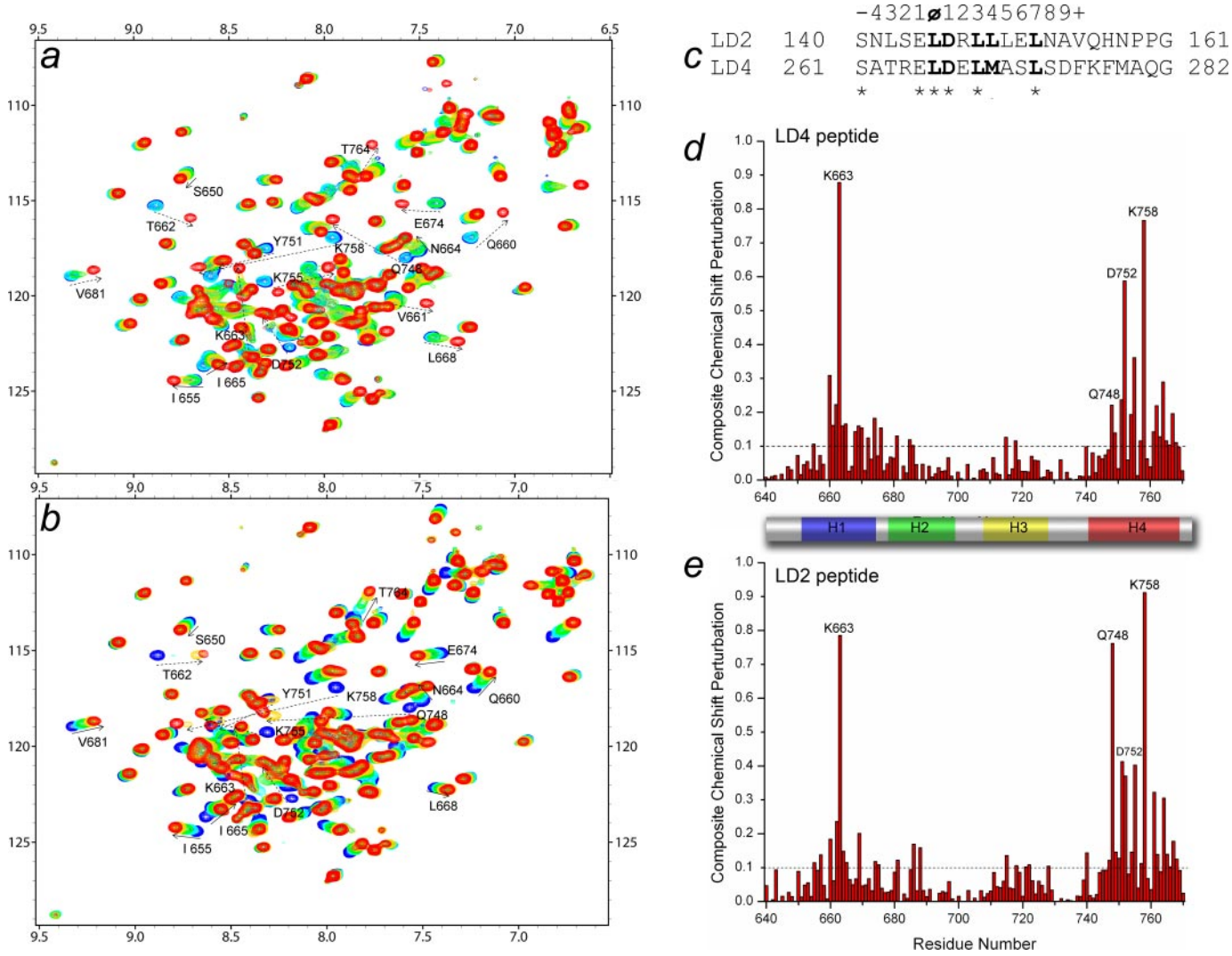

FIGURE 3. **The interaction between the PBD and LD peptides.** *a* and *b*, overlay of GIT1 PBD spectra titrated with LD4 and LD2 peptides, respectively. *Blue*, GIT1 PBD alone; *cyan*, adding 0.5 eq of ligand; *green*, adding 1 eq of ligand; *gold*, adding 2 eq of ligand; *red*, adding 5 eq of ligand. *Arrows* mark significantly perturbed resonance, and *dashed arrows* mark perturbation with intermediate exchange rate. *c*, sequence alignment of human LD2 and LD4 peptides used in this study. Identical residues are marked with *asterisks*, and the LD*X*LL*XX*L motif is shown in *bold*. Conventional nomenclature is used; the first Leu is Φ0, and other residues are named as in the figure. *d* and *e*, composite chemical shift perturbation plotted against residue number for LD4 and LD2, respectively. Composite chemical shift perturbation was calculated by the equation $\Delta\delta_{composite} = (\Delta\delta_{NH}^2 + \Delta\delta_N^2/25)^{1/2}$. Lys^{663}, Lys^{758}, Gln^{748}, and Tyr^{751} are labeled, and they are among those dramatically shifted peaks.

studied the interaction between purified GIT1 PBD and synthesized LD4 peptide with Ser^{272} phosphorylation by NMR chemical shift perturbation experiments. Different from the previous isothermal titration calorimetry data (15), we found the GIT1 PBD spectrum titrated with phosphorylated LD4 peptide (termed as LD4p) was very similar to that of the PBD titrated with the same ratio of LD4 peptide (supplemental Fig. S5), indicating that the two peptides bound to the PBD with similar affinities. Superimposing the ^{15}N HSQC spectra of the PBD mixed with 5 eq of the two peptides revealed that most perturbed peaks could be overlaid (supplemental Fig. S6*a*), suggesting the two peptides bound to the PBD in similar fashions. However, there were clear differences between the two spectra. For example, comparison with the peaks in the spectrum of apo-PBD showed that some peaks were perturbed more by the LD4 binding (supplemental Fig. S6, *b* and *e*), whereas others were perturbed more by the LD4p peptide (supplemental Fig. S6*d*). In addition, the two peptides also shifted some peaks in different directions (supplemental Fig. S6, *c* and *f*). In both cases, either peptide produced consistently larger chemical shift perturbations throughout the PBD binding site, further indicating that the two peptides, LD4 and LD4p, had similar binding affinities to the PBD. These observations suggest that unlike the interaction between the FAT domain of FAK and LD4p (43), in the complex of PBD bound to LD4p peptide, the phosphate group in the peptide has some contacts with the PBD, and those contacts might compensate for the entropy lost due to the phosphorylation (43).

The Binding between the Paxillin LD2 Peptide and the GIT1 PBD—Because the only hydrophobic patch on the GIT1 PBD corresponds to the LD2 motif binding site on the FAT domain of FAK, we investigated whether the LD2 motif also participates in GIT1 binding. Synthesized LD2 peptide (human paxillin 140–161) (Fig. 3*c*) was titrated into uniformly ^{15}N-labeled GIT1 PBD, and the ^{15}N HSQC spectra of the protein during the titration were obtained and examined. Surprisingly, we found

TABLE 2
Binding affinities between GIT1 PBD and LD peptides measured by Biacore binding assay

Interaction	K_d	R_{max}
	μM	RU[a]
GIT + LD2	25.1 ± 0.2	91.0 ± 0.2
GIT + LD4	7.0 ± 0.2	53.3 ± 0.4
GIT + LD4p	9.4 ± 0.2	87.7 ± 0.4

[a] RU, reading units.

that the LD2 peptide also dramatically perturbed the PBD spectrum (Fig. 3*b*), and on average, LD2 binding resulted in a similar change in chemical shift (Fig. 3). Like the LD4 peptide, when the LD2 peptide was titrated into the solution of GIT1 PBD, we found that, in the ^{15}N HSQC spectra of GIT1 PBD, whereas some peaks remained at the same position, many peaks shifted during the titration; some peaks had large shifts, and some even showed intermediate exchange phenomena. Furthermore, in general, LD2 and LD4 binding perturbed the same set of residues, shifting their signals in similar directions and distances. Thus, the LD2 peptide perturbed the GIT1 PBD spectrum to a similar extent as the LD4 peptide, and binding sites of the two peptides overlapped on the H1/H4 surface (Fig. 2*a*).

To determine how the binding occurs with both LD motifs present, we performed competitive titration experiments, in which up to 5 eq of LD2 peptide was titrated into ^{15}N-labeled PBD in the presence of 5 eq of LD4 peptide and vice versa. The competitive experiments agreed with the single-peptide titration data, confirming that each peptide was able to further perturb the spectrum in the presence of an equal concentration of the other peptide (supplemental Fig. S7). The two final spectra overlaid well, indicating that the binding reaches equilibrium regardless of the order in which the peptides were added. It is likely that both peptides compete for the same binding site with similar affinity, and the concentration of available LD motifs may dynamically determine the equilibrium state.

To test the binding between PBD and paxillin, we titrated the PBD with up to 5 eq of chicken paxillin 133–288, which contains both LD2 and LD4 motifs. The spectrum of PBD titrated with 5 eq of paxillin 133–288 overlaid well with the PBD spectrum titrated with 5 eq of both LD2 and LD4 peptides, exhibiting an average of binding from both LD motifs (supplemental Fig. S8). It also showed that the LD3 motif, which was also present in the paxillin construct, did not interact with GIT1 PBD.

Examining the Interactions between LD Peptides and GIT1 PBD by Biacore Binding Studies—To further characterize the binding properties of the two paxillin peptides to the PBD, we measured the binding affinities between the LD peptides and the PBD by the Biacore binding assay. In the experiments, the LD peptides were synthesized with an N-terminal biotin tag connected with a flexible GGSG linker. The peptides were immobilized on a NeutrAvidin-coated chip and run through the purified GIT1 PBD protein. As summarized in Table 2, the PBD bound to the LD4 peptide with a K_d of 7.2 μM, which is close to the reported K_d of 10 μM (15). The LD2 peptide showed a slightly higher K_d of 25.1 μM. Because the LD2 peptide binds to the GIT1 PBD with a K_d only about three times weaker than the LD4 peptide, the two peptides should be able to compete for the ligand binding site on the surface of the PBD, and indeed this conclusion is in agreement with our NMR experiments. Also consistent with our NMR studies, the assays showed that the binding affinity of the LD4p peptide, the LD4 peptide with Ser^{272} phosphorylation, to the PBD increased only slightly to a K_d value of 10.2 μM.

DISCUSSION

The solution structure of the GIT1 PBD is a stable four-helix bundle, which is similar to the structures of the FAT domain of FAK and the Vt domain. The structure was validated by the solvent exposure surface mapped by the H/D exchange experiment. The PBD forms an up-and-down helix bundle with an average axis angle of 19.1°, which is close to the ideal antiparallel helix packing angle of 20° (44). The PBD, the FAT domain of FAK, and the Vt domain share a well conserved hydrophobic core, but their surface residues exhibit more diversity. This explains the very similar overall folding of the three domains as well as their distinct binding specificity.

Both the PBD and the FAT domain interact with the LD2 and LD4 motifs of paxillin and are responsible for targeting GIT1 and FAK to focal adhesions. However, there are distinct differences between the two domains. First, in solution, the FAT domain forms a dimer by swapping H1 between the two protomers (25), whereas the PBD is a well folded monomer. Second, the LD2 and LD4 motifs of paxillin interact with the FAT domain simultaneously at two opposite faces of the four-helix bundle (45, 46), whereas the LD2 and LD4 motifs of paxillin bind to the PBD at the same site, the H1/H4 site. These functional differences between the FAT domain and the PBD are rooted in the difference of their sequences.

The previously reported interaction between the LD4 motif of paxillin and the GIT1 PBD (11, 13, 14) was confirmed in our studies. The binding site mapped by NMR was also in agreement with the recent mutation study (15), in which all residues critical for LD4 binding exhibited strong chemical shift perturbation. The LD4 motif binds to the H1/H4 site of the PBD, unlike the complex of LD4 with the FAT domain of FAK, where it binds to the H2 and H3 surface. This variation may also explain another difference between the two complexes: although Ser^{272} phosphorylation within the LD4 motif decreases LD4 binding to the FAT domain (43), the LD4 Ser^{272} phosphorylated peptide, LD4p, interacts with the PBD similarly to the LD4 peptide.

It has been proposed that paxillin Ser^{272} phosphorylation is an important event in focal adhesion regulation (11, 12, 43). In a working model, FAK and GIT1 compete for paxillin binding, and, in turn, the two proteins compete for FA localization. When paxillin Ser^{272} is dephosphorylated, paxillin prefers binding to FAK because FAK binds both the paxillin LD2 and LD4 motifs cooperatively with a higher affinity. Once Ser^{272} is phosphorylated, the affinity between LD4 and FAK is weakened, causing disassociation of FAK-LD4 (43). However, the phosphorylation of Ser^{272} in LD4 does not affect the interaction between paxillin and GIT1. Therefore, paxillin Ser^{272} phosphorylation shifts the balance of the paxillin interaction with FAK *versus* GIT1 in favor of GIT1 and causes an increase in the paxillin·GIT1 complex. This would decrease FAK while

increasing PAK (through GIT1) in the FAs. Because FAK has been linked to FA assembly, and PAK can promote FA disassembly (11, 12, 43), this shifting balance may promote regulated FA assembly and disassembly.

The FAT domain of FAK binds to paxillin by interacting with both the paxillin LD2 and LD4 motifs simultaneously using its H1/H4 and H2/H3 sites (45, 46). With two binding sites, the FAT domain should have a much stronger binding affinity with paxillin than the GIT1 PBD because the PBD has only one LD binding site, the H1/H4 site. This concern can be alleviated by another novel finding in this work: the paxillin LD2 motif also interacted with the GIT1 PBD. Because the LD2 motif binds to the PBD as well, GIT1 might achieve a binding affinity comparable with FAK by interacting with both the LD2 and LD4 motifs of paxillin. Indeed, in our studies, we not only showed that the LD2 motif of paxillin could bind to the GIT1 PBD, but in one experiment we also found that the spectrum of the PBD bound with paxillin 133–288, which contained both the LD2 and LD4 motifs, was an average of the spectra of the PBD bound with the LD2 and LD4 peptides (supplemental Fig. S8). Furthermore, such observation did not change even when the paxillin concentration was increased to five times that of the PBD, indicating that the two LD motifs have similar affinity to the PBD and bind GIT1 simultaneously. In other words, it suggests that one paxillin can bind two GIT1 proteins. Conversely, GIT1 can dimerize in solution through its central coiled-coil domain (47). Considering the length of the flexible linker between the LD2 and LD4 motifs, it is possible that two GIT1 proteins in a dimer can bind to one paxillin molecule simultaneously, through both the LD2 and LD4 motifs. Indeed, GIT1 is found primarily as an oligomer together with PIX (47, 48), and the oligomerization is essential for GIT1 FA localization (49, 50).

Acknowledgments—We appreciate the gift of rat GIT1 full-length cDNA from Dr. Edward Manser (Institute of Molecular and Cell Biology, Singapore). We thank Dr. Craig M. Bertolucci for constructive suggestions. We thank Dr. Brett Waddell for the Biacore binding study and Dr. Patrick Rodrigues for peptide synthesis at the Hartwell Center of Bioinformatics and Biotechnology, St. Jude Children's Research Hospital, Memphis, TN. We thank Dr. Vani Shanker from Scientific Editing for editorial help. We also thank Drs. Weixing Zhang and Charles Ross for support to the NMR instruments and computer resources. We thank GE Healthcare for loaning the Biacore instrument.

REFERENCES

1. Jockusch, B. M., Bubeck, P., Giehl, K., Kroemker, M., Moschner, J., Rothkegel, M., Rudiger, M., Schluter, K., Stanke, G., and Winkler, J. (1995) *Annu. Rev. Cell Dev. Biol.* **11,** 379–416
2. Sastry, S. K., and Burridge, K. (2000) *Exp. Cell Res.* **261,** 25–36
3. Sastry, S. K., Lakonishok, M., Wu, S., Truong, T. Q., Huttenlocher, A., Turner, C. E., and Horwitz, A. F. (1999) *J. Cell Biol.* **144,** 1295–1309
4. Ilic, D., Almeida, E. A., Schlaepfer, D. D., Dazin, P., Aizawa, S., and Damsky, C. H. (1998) *J. Cell Biol.* **143,** 547–560
5. Cary, L. A., and Guan, J. L. (1999) *Front. Biosci.* **4,** D102–D113
6. Premont, R. T., Claing, A., Vitale, N., Freeman, J. L., Pitcher, J. A., Patton, W. A., Moss, J., Vaughan, M., and Lefkowitz, R. J. (1998) *Proc. Natl. Acad. Sci. U. S. A.* **95,** 14082–14087
7. Manser, E., Leung, T., Salihuddin, H., Zhao, Z. S., and Lim, L. (1994) *Nature* **367,** 40–46
8. Ridley, A. J., and Hall, A. (1992) *Cell* **70,** 389–399
9. Ridley, A. J., Paterson, H. F., Johnston, C. L., Diekmann, D., and Hall, A. (1992) *Cell* **70,** 401–410
10. Nobes, C. D., and Hall, A. (1995) *Biochem. Soc. Trans.* **23,** 456–459
11. Zhao, Z. S., Manser, E., Loo, T. H., and Lim, L. (2000) *Mol. Cell. Biol.* **20,** 6354–6363
12. Nayal, A., Webb, D. J., Brown, C. M., Schaefer, E. M., Vicente-Manzanares, M., and Horwitz, A. R. (2006) *J. Cell Biol.* **173,** 587–589
13. Turner, C. E., Brown, M. C., Perrotta, J. A., Riedy, M. C., Nikolopoulos, S. N., McDonald, A. R., Bagrodia, S., Thomas, S., and Leventhal, P. S. (1999) *J. Cell Biol.* **145,** 851–863
14. West, K. A., Zhang, H., Brown, M. C., Nikolopoulos, S. N., Riedy, M. C., Horwitz, A. F., and Turner, C. E. (2001) *J. Cell Biol.* **154,** 161–176
15. Schmalzigaug, R., Garron, M. L., Roseman, J. T., Xing, Y., Davidson, C. E., Arold, S. T., and Premont, R. T. (2007) *Cell. Signal.* **19,** 1733–1744
16. Bagrodia, S., Bailey, D., Lenard, Z., Hart, M., Guan, J. L., Premont, R. T., Taylor, S. J., and Cerione, R. A. (1999) *J. Biol. Chem.* **274,** 22393–22400
17. Hoefen, R. J., and Berk, B. C. (2006) *J. Cell Sci.* **119,** 1469–1475
18. Brown, M. C., and Turner, C. E. (2004) *Physiol. Rev.* **84,** 1315–1339
19. Brown, M. C., Curtis, M. S., and Turner, C. E. (1998) *Nat. Struct. Biol.* **5,** 677–678
20. Dawid, I. B., Breen, J. J., and Toyama, R. (1998) *Trends Genet.* **14,** 156–162
21. Nikolopoulos, S. N., and Turner, C. E. (2000) *J. Cell Biol.* **151,** 1435–1448
22. Nikolopoulos, S. N., and Turner, C. E. (2001) *J. Biol. Chem.* **276,** 23499–23505
23. Brown, M. C., Perrotta, J. A., and Turner, C. E. (1996) *J. Cell Biol.* **135,** 1109–1123
24. Liu, G., Guibao, C. D., and Zheng, J. (2002) *Mol. Cell. Biol.* **22,** 2751–2760
25. Arold, S. T., Hoellerer, M. K., and Noble, M. E. (2002) *Structure* (*Camb.*) **10,** 319–327
26. Thomas, J. W., Cooley, M. A., Broome, J. M., Salgia, R., Griffin, J. D., Lombardo, C. R., and Schaller, M. D. (1999) *J. Biol. Chem.* **274,** 36684–36692
27. Neidhardt, F. C., Bloch, P. L., and Smith, D. F. (1974) *J. Bacteriol.* **119,** 736–747
28. Goddard, T. D., and Kneller, D. G. *SPARKY 3*, University of California, San Francisco, CA
29. Delaglio, F., Grzesiek, S., Vuister, G. W., Zhu, G., Pfeifer, J., and Bax, A. (1995) *J. Biomol. NMR* **6,** 277–293
30. Keller, R. (2004) *The Computer Aided Resonance Assignment Tutorial*, 1st Ed., Verlag, Cantina, Switzerland
31. Cornilescu, G., Delaglio, F., and Bax, A. (1999) *J. Biomol. NMR* **13,** 289–302
32. Herrmann, T., Guntert, P., and Wuthrich, K. (2002) *J. Biomol. NMR* **24,** 171–189
33. Herrmann, T., Guntert, P., and Wuthrich, K. (2002) *J. Mol. Biol.* **319,** 209–227
34. Guntert, P. (1998) *Q. Rev. Biophys.* **31,** 145–237
35. Laskowski, R., MacArthur, M., Moss, D., and Thornton, J. (1993) *J. Appl. Crystallogr.* **26,** 283–291
36. Koradi, R., Billeter, M., and Wuthrich, K. (1996) *J. Mol. Graph. Model.* **14,** 29–32, 51–55
37. Nicholls, A., Sharp, K. A., and Honig, B. (1991) *Proteins* **11,** 281–296
38. Guex, N., and Peitsch, M. C. (1997) *Electrophoresis* **18,** 2714–2723
39. Sharma, D., and Rajarathnam, K. (2000) *J. Biomol. NMR* **18,** 165–171
40. Prutzman, K. C., Gao, G., King, M. L., Iyer, V. V., Mueller, G. A., Schaller, M. D., and Campbell, S. L. (2004) *Structure* (*Camb.*) **12,** 881–891
41. Hoellerer, M. K., Noble, M. E., Labesse, G., Campbell, I. D., Werner, J. M., and Arold, S. T. (2003) *Structure* (*Camb.*) **11,** 1207–1217
42. Brown, M. C., West, K. A., and Turner, C. E. (2002) *Mol. Biol. Cell* **13,** 1550–1565
43. Bertolucci, C. M., Guibao, C. D., and Zheng, J. J. (2008) *Biochemistry* **47,** 548–554
44. Chothia, C., Levitt, M., and Richardson, D. (1981) *J. Mol. Biol.* **145,**

215–250
45. Bertolucci, C. M., Guibao, C. D., and Zheng, J. (2005) *Protein Sci.* **14,** 644–652
46. Hayashi, I., Vuori, K., and Liddington, R. C. (2002) *Nat. Struct. Biol.* **9,** 101–106
47. Paris, S., Longhi, R., Santambrogio, P., and de Curtis, I. (2003) *Biochem. J.* **372,** 391–398
48. Premont, R. T., Perry, S. J., Schmalzigaug, R., Roseman, J. T., Xing, Y., and Claing, A. (2004) *Cell. Signal.* **16,** 1001–1011
49. Kim, S., Lee, S. H., and Park, D. (2001) *J. Biol. Chem.* **276,** 10581–10584
50. Loo, T. H., Ng, Y. W., Lim, L., and Manser, E. (2004) *Mol. Cell. Biol.* **24,** 3849–3859